Characteristic analysis of electromagnetic acoustic transducers for helical shear horizontal wave based on magnetostrictive effect

S.L. Huang[1], Z. Wang[1], S. Wang[1], Q. Wang[2] and W. Zhao[1]

1. State Key Laboratory of Power System, Department of Electrical Engineering, Tsinghua University, Beijing, 100084, China.
2. Department of Engineering, Durham University, Durham, DH1 3LE, United Kingdom

The electromagnetic ultrasound detection technology provides an efficient method to inspect the structural health status. For the pipeline structure, the guided ultrasonic wave propagating along the axial direction has been the focus of the current research. However, the helical wave owns the advantage of obtaining the defect information in extra angles and has not been explored sufficiently. In this work, a transducer with a sector configuration is designed for generating helical shear horizontal waves in a pipeline. The magnetostrictive effect is analyzed, and the model is built in the finite element simulation software of COMSOL Multiphysics. The electromagnetic field and displacement distribution are studied. To evaluate the performance of the transducer, the half divergence angle is defined to measure the acoustic beam and evaluate the capacity in generating helical waves. Corresponding experiments are also implemented to analyze the influencing factors in the structural design of the transducer. The results indicate that the pulse cycle affects the half divergence angle slightly. The compromise should be considered when designing the central angle of the transducer because it influences the signal amplitude and further imaging resolution in a contradictory way.

I. INTRODUCTION

The pipe structure can transport fluid materials efficiently. In particular, long-distance pipelines made of ferromagnetic materials play a vital role in the task of transporting oil and gas resources.[1] In the long-term service of the pipeline, aging and corrosion will inevitably occur.[2,3] Once the oil or gas leaks, it will often cause huge economic losses and also damage the ecological environment. Therefore, regular inspection of pipelines is significant in ensuring the energy security, protecting the natural environment, and maintaining the safety of property.[4–7]

The non-destructive testing methods have been extensively used for structural inspection.[8–10] The common methods include ultrasonic testing, eddy current testing, magnetic flux leakage, and radiographic testing. The method of electromagnetic ultrasonic wave detection can overcome the shortcomings of the coupling agent required in traditional ultrasonic wave testing.[11] It has the advantages of non-contact, long-range, and large-scale detection.[12,13] The Electromagnetic Acoustic Transducer (EMAT) can excite multiple types of guided ultrasonic waves in the pipeline, including guided circumferential waves, guided longitudinal waves, and guided helical waves. Furthermore, the guided circumferential wave can be subdivided into the guided circumferential Lamb wave and guided circumferential shear horizontal (SH) wave.[14,15]

The vibration mode of the SH wave is simple, and it is easy to be generated by using the EMAT. Zhao and Rose numerically solved the dispersion curve of the guided circumferential SH wave and analyzed the displacement wave structure.[15] Wang et al. performed 3D simulation of the circumferential SH guided wave and interaction of waves with defects.[16] Luo et al. arranged a magnetostrictive sensor on the outer wall of the pipeline to excite the circumferential SH guided wave in pipelines with defects of different depths and lengths.[17,18] Hirao and Ogi placed a periodic-permanentmagnet (PPM) EMAT on the inner wall of the pipeline and used the circumferential SH guided wave to detect corrosion defects on the outer wall of the pipeline.[19]

The guided circumferential SH wave is more sensitive to axial cracks existing in the pipeline. However, the guided helical SH wave propagating along the spiral line can detect both axial and circumferential defects on the pipeline simultaneously. Kim et al. used segmented magnetostrictive patches to successfully generate helical SH waves propagating spirally along the surface of a hollow cylinder.[20] Furthermore, they designed a transducer structure including a permanent magnet, a figure-of-eight coil, and a magnetostrictive patch.[21] The wide-directional spiral-propagating SH wave was excited in the pipeline, and its energy was mainly concentrated in the circumferential direction. However, the design of EMATs is rather complicated. In addition, up to now, the wave propagating in the helical direction requires further investigation and the characteristic analysis of the transducer does not attract sufficient attention.

The energy conversion process in the EMAT involves the mutual coupling of multiple physical fields.[22–24] Therefore, it is difficult to obtain exact analytical expressions. The early EMAT design and optimization required a lot of physical experiments, which was time-consuming and often failed to achieve ideal results. With the improvement of computer performance and numerical simulation algorithms, the finite element analysis provides a solution for simulation, which accelerates the process and becomes an important tool for scientific research. In the 1970s, Thompson established models of electromagnetic ultrasonic surface wave transducers and Lamb wave transducers.[25] Ogi used a numerical simulation method to explore the relationship between the static magnetic field and the EMAT efficiency.[26] Wan et al. established a model to quantitatively evaluate the simulation accuracy and select appropriate finite element size and time step.[27]

In view of the research about helical guided wave so far, this work proposes a newly designed transducer with simple structure for generating helical SH wave in pipelines. The magnetostrictive effect is applied and the transducer is composed of iron-nickel alloy belt, magnetic poles and copper wire. The theoretical model is established and the finite element simulation is conducted to analyze the displacement distribution in the pipeline. The half divergence angle is defined to evaluate the ability to generate helical wave. The working principle is also verified in the experiment. In addition, the factors influencing the transduction process are analyzed aiming to provide instructions when applying the designed transducer.

II. THEORETICAL ANALYSIS

The inspection method based on the EMAT can be coupled to an object without using coupling agents such as glycerin. Therefore, defect detection can be performed efficiently by getting rid of complicated cleaning of the pipeline surface. The EMAT is generally composed of coils, permanent magnets, and objects to be detected. The process involves a multiphysics problem including an electromagnetic field, force field, and sound field. Based on the Lorentz force and the magnetostrictive effect, the guided wave is generated. In this work, the latter principle is investigated and utilized to generate helical SH waves in the pipeline.

The magnetostrictive effect occurs only in ferromagnetic materials. Due to the magnetization, the objects made of ferromagnetic materials will generate tiny deformation.[28] The process opposite to magnetostriction is called the inverse magnetostrictive effect. It was thought that the magnetostrictive constitutive relationship was linear at earlier time. Thompson used the piezomagnetic equation to describe the forcemagnetic coupling relationship.[29] Sablik and Rubin derived and analyzed the wave equations that characterize the magnetostrictive effect.[30,31] Due to the magnetization nonlinearity of ferromagnetic materials and the difficulty of carrying out corresponding experiments, the study of this mechanism needs to be further explored.

The existing theory believes that there are many small magnetic domains inside ferromagnetic materials. If no external magnetic field is applied, the orientation of these small magnetic domains is random, and the magnetic fields generated by them cancel each other out. Thus, they do not show magnetism to the outside object. When the static magnetic field is applied to them, the magnetic domains rotate along the direction of the outer magnetic field. This will cause a small change in the volume or length of the ferromagnetic material. When a dynamic magnetic field is applied to the ferromagnetic material, the magnetic domains are repeatedly deflected. It will lead to local vibration of the material and excite ultrasonic waves.

The magnetostrictive effect can be modeled approximately as the linear piezomagnetic equation,

$$\varepsilon = s^H \sigma + dH, \tag{1}$$

$$B = d^T \sigma + \mu^\sigma H, \tag{2}$$

where ε is strain, σ is stress, H is the magnetic field intensity, B is the magnetic flux density, d is the piezomagnetic coefficient matrix, d^T is the transpose of d, s^H is the elastic compliance matrix under constant H, and μ^σ is the magnetic permeability matrix under constant σ.

The common structure of the EMAT currently used for guided SH waves is shown in Fig. 1. The magnets are used to provide a static magnetic field or bias magnetic field. The coil is activated with alternating pulse current to generate a dynamic magnetic field.

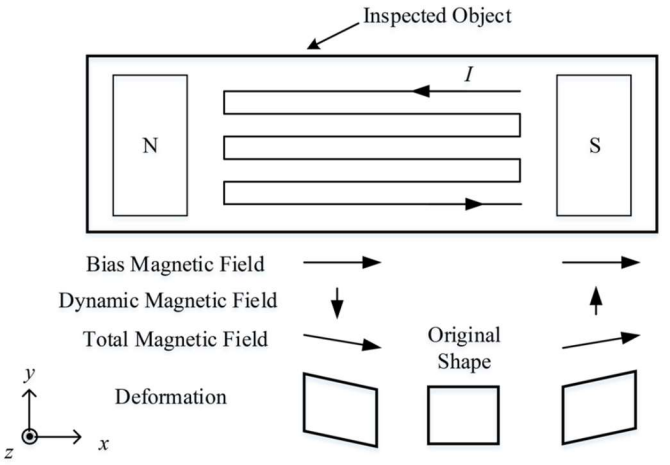

Fig.1: The common structure of the EMAT for guided SH waves based on the magnetostrictive effect.

In this case, the dynamic magnetic field is perpendicular to the static magnetic field. The direction of elongation and contraction of the ferromagnetic material is also perpendicular to that of the bias magnetic field. Thus, the guided SH wave is generated.

The magnetostrictive force f_M can be derived from the linear piezomagnetic equation.[32] Its expression is described as follows:

$$f_M = -2(1+\nu)c_{66}\frac{\varepsilon_6}{H_x}\frac{\partial H_y}{\partial y}, \tag{3}$$

where c_{66} is the element in the elastic stiffness matrix, ε_6 is the element in strain, ν is Poisson's ratio, and Hx and Hy are the components of magnetic field intensity. Under the imposition of magnetostrictive force, vibration occurs and propagates along the structure to form the guided SH wave.

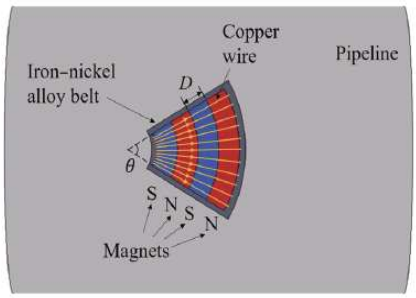

(a)

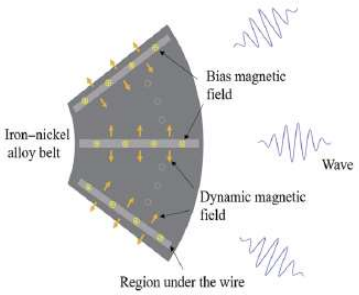

(b)

FIG. 2. The illustration of the proposed EMAT for the helical guided SH wave. (a) The structure of the designed transducer. (b) The representation of the magnetic fields and waves.

III. DESIGN OF THE DEVELOPED EMAT

In this work, the helical guided SH wave is investigated. Many researchers have compared the guided waves in a pipeline with waves in a flat plate. The helical guided SH wave propagates along the pipeline with a helix angle, which looks like it propagates in a curved plate. The helical guided wave can propagate along the pipeline from more angles than the guided wave propagating only along the axial direction. Therefore, the helical guided SH wave is capable of obtaining more defect information about the inspected pipeline. Thus, more accurate pipeline defect diagnosis could be achieved. The designed structure of the transducer is depicted in Fig. 2(a). This EMAT contains multiple magnetic poles, wound copper wire, and an iron-nickel alloy belt. The illustration of the magnetic fields is also shown in Fig. 2(b). The dynamic magnetic field from the current in the wire is perpendicular to the bias magnetic field from the magnets. Thus, the shear deformation will occur to produce the helical guided SH wave.

The iron–nickel alloy belt is adopted because it owns high magnetostriction. The belt is tightly wound around the outer wall of the pipe. The magnetostrictive effect is utilized, and the belt works as the force source. The magnets are placed above the iron–nickel alloy belt with a certain lift-off distance. The magnets present the shape of the sector with the central angle of θ. The structure is developed to make it more suitable to generate helical waves. The copper wire is wound around the magnets, and the wire is connected to the outer pulse source. The transducer only covers part of the pipeline so that multiple transducers can be arranged to form an array. The width D of each magnetic pole satisfies

$$D = \frac{1}{2}\lambda, \tag{4}$$

where λ is the wavelength. Through fixing the width parameter, the corresponding wavelength is superposed positively in the generated wave, while the others are suppressed. In order to reduce the effect of the dispersion effect, the excitation pulse flowing through the wire is set as a tone-burst signal. The tone-burst signal owns a narrow

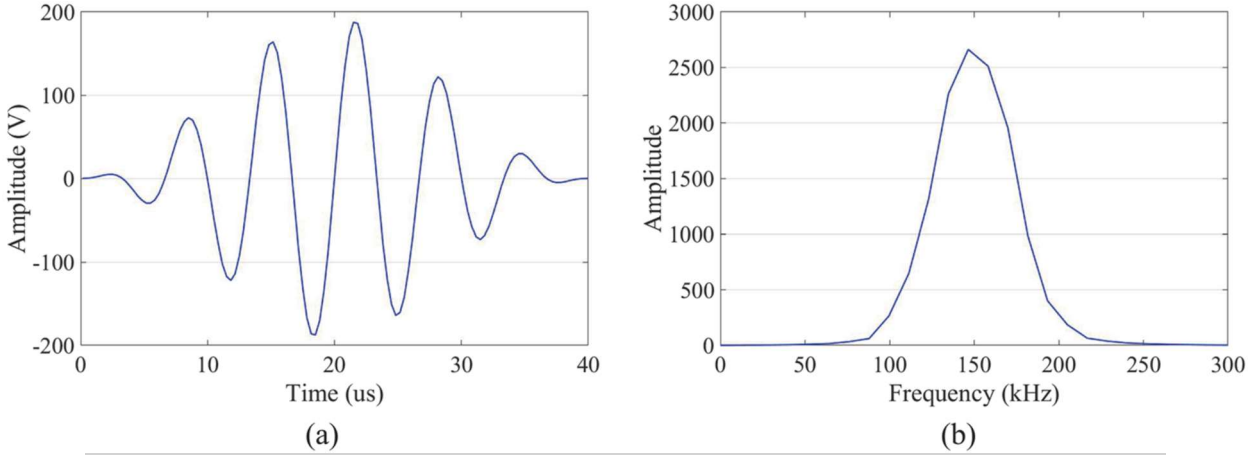

(a) (b)

Fig.3: Representation of the excitation pulse. (a) The waveform of the tone-burst. (b) The corresponding spectrum.

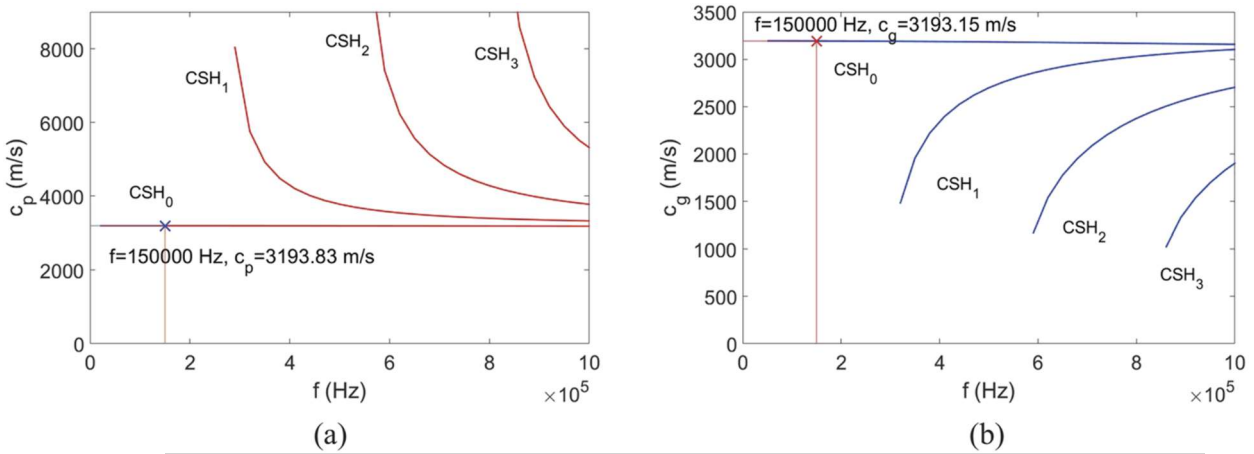

Fig.4: Dispersion curve for the circumferential guided SH wave. (a) The phase velocity. (b) The group velocity.

Bandwidth, and it can be expressed as

$$I = \frac{1}{2}A\left[(H_e(t)) - H_e\left(t - \frac{N}{f_c}\right)\right]\sin(2\pi f_c)\left(1 - \cos\frac{2\pi f_c t}{N}\right), \quad (5)$$

where A is the amplitude of the excitation signal, $H_e(t)$ is the Heaviside step function, N is the cycle number of the excitation signal, and f_c is the center frequency. The waveform and corresponding spectrum of the tone-burst signal are shown in Fig. 3. It can be seen that the center frequency of 150 kHz is in the middle of the spectrum and owns the highest value. This tone-burst is generated by the arbitrary waveform generator and further exemplified by the power source. The transducer with the same structure is used as the wave receiver according to the inverse magnetostrictive effect. The signal is then amplified and collected for the following analysis

The helical SH wave propagates around the pipeline in a spiral path with a constant curvature, which can be equivalently regarded as the circumferential guided SH wave with the same curvature.[20] Combining the elastodynamics equation with boundary conditions, the dispersion curve can be obtained. Figure 4 shows the dispersion curve of the circumferential SH wave in a pipeline with an outer diameter of 273mm and thickness of 6 mm.

From the dispersion curve, it can be seen that the dispersion phenomenon barely occurs in the low-order mode. The phase velocity is independent of the frequency and remains at 3193.83 m/s. Therefore, this mode should be used to inspect pipeline defects. The relation of wave velocity and frequency can be expressed as

$$c_p = f\lambda, \quad (6)$$

where f is the frequency and cp is the phase velocity. The wavelength is influenced by the parameter of magnets. In this work, the width D of 10.7mm is chosen and, then, the corresponding wavelength is 21.4 mm. According to the relation in (6), the frequency should be 150 kHz, which is also the center frequency of the excitation pulse. In addition, under this frequency, no higher-order mode exists. This is undoubtedly easier for subsequent extraction and analysis of signal information.

IV. VERIFICATION AND ANALYSIS OF THE TRANSDUCER

A. Finite element simulation

The finite element method is first used to analyze the developed helical guided SH wave transducer. The stress, strain, and displacement that occurred in the pipeline will be observed. The simulation is performed using the commercial finite element software of COMSOL Multiphysics. This software provides the solution for multiphysics modeling, which is suitable for solving Multiphysics problems in EMATs. The EMAT simulation involves electromagnetic and force fields. The modules used in this work include the AC/DC Module and Structural Mechanics Module.

The parameters used in the helical guided SH wave model are listed in Table I. The copper wire with a sectional area of 6mm^2 is used, and it is wrapped around the magnetic poles with 11 turns. The iron–nickel alloy belt has the thickness of 1 mm. The residual magnetic flux density of the magnet is 0.6 T. In electromagnetic fields, the excitation pulse is loaded on the wire, which generates the dynamic magnetic field in the iron–nickel alloy belt and pipeline. In the displacement field, the two ends of the pipeline are set as low-reflection boundaries to reduce the influence of the boundary reflection on the received signal. In order to ensure the accuracy of the simulation results and reduce the time assumption, the meshing size follows the principle given as follows:

$$\Delta(x) < \frac{\lambda}{10}, \quad (7)$$

TABLE I. Parameters of the iron-nickel alloy belt and pipeline

Material	Density (kg m^{-3})	Young's modulus (Pa)	Poisson's ratio	Relative permeability
Pipeline	7850	205 x 10^9	0.28	150
Iron-nickel alloy belt	8880	207 x 10^9	0.31	250

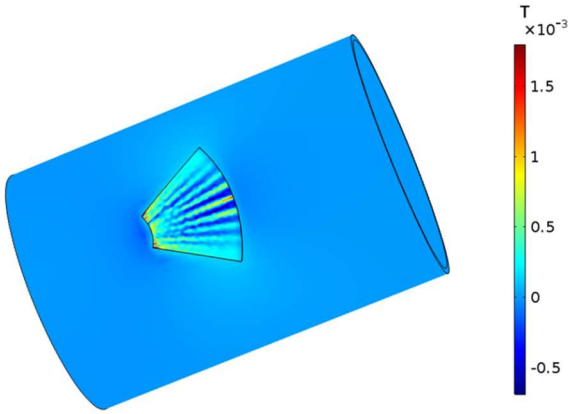

Fig.5: The dynamic magnetic field generated by the excitation pulse at 12 μs .

where Δ(x) is the size of the mesh in the simulation. Because it is required to observe the propagation of the helical guided SH wave over time, the time transient analysis is applied.

The results of the dynamic magnetic field in the belt at 12 μs are presented in Fig. 5. It can be seen that the magnetic field is in the shape of wound wire and concentrated in the regions under the wire.

The displacement of the pipeline at 18 μs is shown in Fig. 6. The main direction of the acoustic beam is parallel to the axial direction of the pipe. The wave also spreads outward and forms a certain angle with the pipeline axis. To analyze the radiation pattern, the half divergence angle of the acoustic beam α is defined to describe the extent of the energy concentration.

The calculation of α can be expressed as follows:

$$\tan \alpha = \frac{l}{C}, \tag{8}$$

where C is the circumferential length of the pipeline and l is the half distance where the normalized amplitude is larger than 0.6. Figure 7 provides the illustration for the concept of half divergence angle. The criterion of amplitude is readily accessible to measure the performance of the transducer.

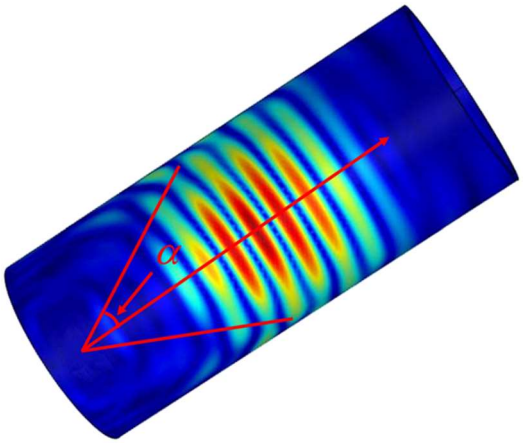

Fig.6: The displacement that occurred in the pipeline at 18 μs .

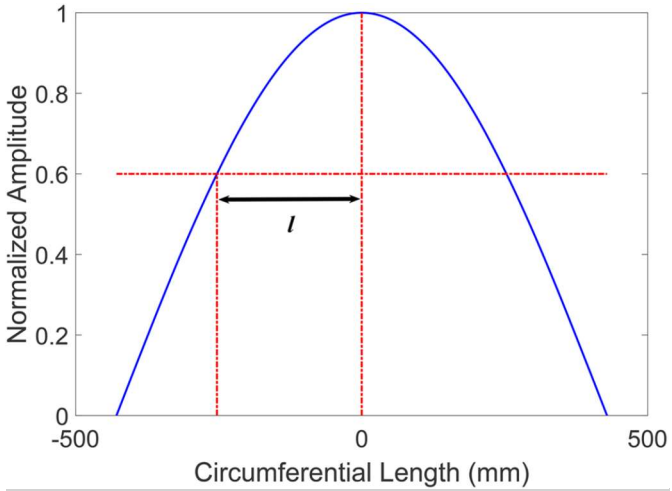

Fig.7: The illustration to understand the defined half divergence angle.

The larger α means that more energy is dispersed, and more energy is obtained in the circumferential direction. Thus, it is easier to generate helical guided waves. Therefore, the optimization objective can be expressed as max α.

Therefore, in the next part, the influencing factors for the transducer are analyzed to obtain the divergence angle.

B. Experimental setup and procedure

To verify the results obtained in the simulation, the experimental investigations are also performed. The pitch-catch approach is used, and the schematic diagram of the experimental setup is depicted in Fig. 8. The arbitrary waveform generator is adopted to produce the excitation pulse. Then, the pulse is amplified by the high power pulser of RITEC RPR-4000. The cables from the pulse output are connected first to an impedance matching box, which is composed of multiple resistors and capacitors to adjust the excitation power.

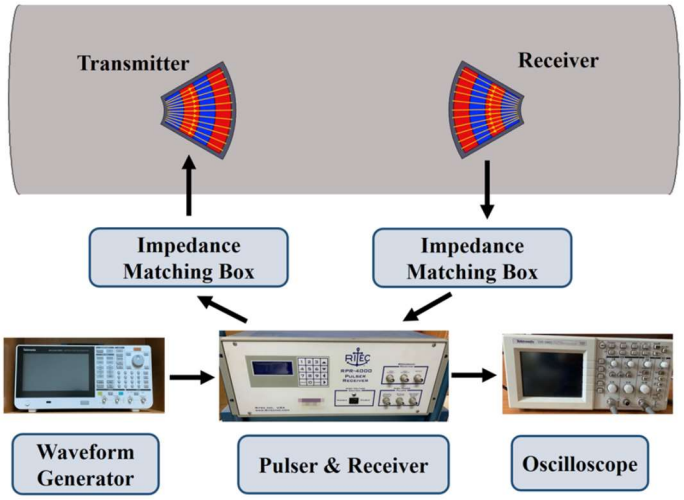

Fig. 8: The schematic diagram of the experimental setup.

The transmitter is connected to the output of the impedance matching box. The receiver is set in a distance with the transmitter to receive the generated guided wave. In this work, the receiver is not fixed and can be moved in the axial and circumferential direction along the pipeline to detect the guided wave. Thus, the performance of the designed transducer can be further analyzed quantitatively in the experiments.

The pipeline tested in this work owns the outer radius of 273mm and thickness of 6 mm. This size of the pipeline is used in the practical oil transport project. The waveform from the receiver along a line in front of the transmitter is presented in Fig. 9. The distance between the receiver and the transmitter is 300 mm. The waveform from the simulation is also provided. To better compare the results in the simulation and experiment, the amplitude is adjusted to the range from −1 to 1. It is worth noting that the two waveforms are in agreement with each other but with a small discrepancy. The error of the property of the pipeline specimen and the error in the manufacturing of the transducer contribute to the discrepancy.

C. Characteristic analysis

1. Frequency response characteristics

One pair of developed transducers is installed on the outer surface of the pipeline. The frequency response is first carried out in the experiment to verify the theory of the working principle. In the design of this transducer, the center frequency that matched the geometric parameters of the magnets is 150 kHz. To obtain the actual frequency of the EMAT, the excitation frequency of the pulse varied from 50 kHz to 250 kHz. The frequency increment is set as 10 kHz. The pulse cycle number remains 6 in this test. The results of frequency response characteristics are presented in Fig. 10. The curve fitting technique is adopted to deal with the discrete points. Thus, the calculated center frequency is 146 kHz, which owns the maximum wave amplitude. Then, the relative error between the actual and designed frequency is 2.67%. The error is acceptable considering the discrepancy existing in the material property and transducer manufacturing.

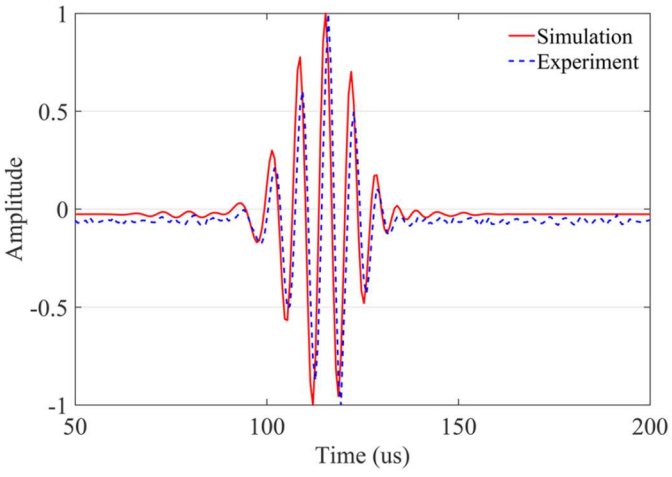

Fig. 9: The received waveform in the simulation and experiment. The amplitudes are normalized to compare the results.

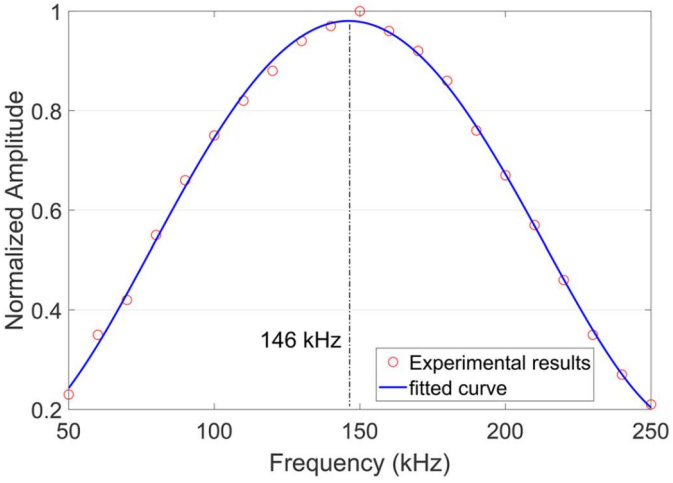

Fig. 10: The frequency response characteristics of the designed transducer.

2. Lift-off distance

There exists a lift-off distance between the magnets and iron–nickel alloy belt. However, the lift-off is one of the important factors affecting the performance of the EMAT. Using different liftoff values, the magnetic field intensity in the iron–nickel alloy belt is shown in Fig. 11. The results are obtained in the simulation to control the distance accurately. It can be seen that the maximum value of the magnetic field intensity decays exponentially with the increase in the lift-off distance. Therefore, when designing the EMAT for a helical SH guided wave, the lift-off value should be reduced as much as possible to bring the coil closer to the detected object. The approximate relationship between the magnetic field intensity and the lift-off distance is fitted using the least squares method. The fitting results are shown in Fig. 12.

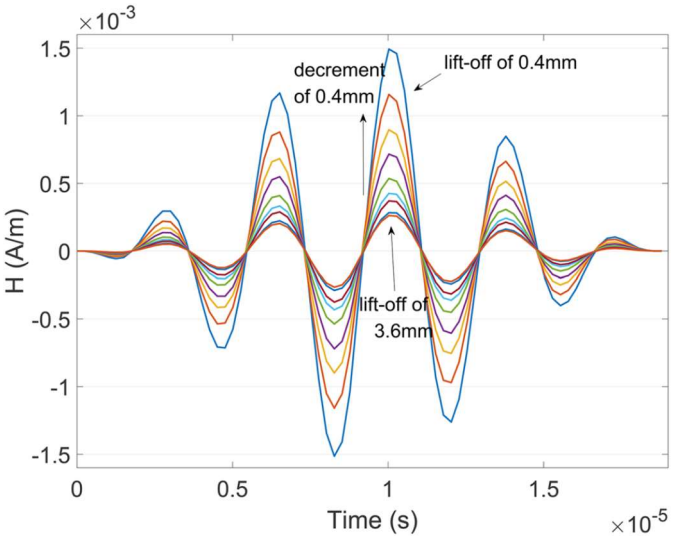

Fig. 11: The magnetic field intensity obtained in the iron-nickel alloy belt under different lift-off conditions.

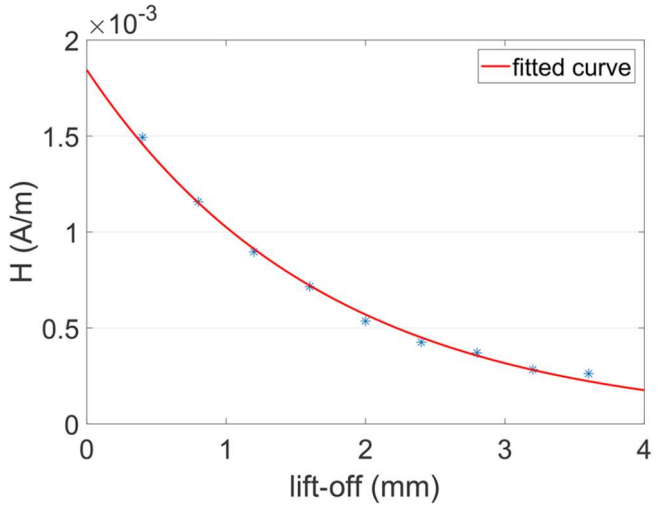

Fig. 12: The lift-off distance and magnetic field intensity are fitted using an exponential relation.

The relation can be expressed as

$$H_{\max} = 0.0018 \cdot e^{-0.58 d_l}, \quad (9)$$

where d_l is the lift-off distance and *Hmax* is the maximum value of the magnetic field intensity. From the fitting effect, it can be seen that the error in the fitting process is rather small.

3. Number of excitation pulse cycles

The excitation pulse is formed by using the arbitrary waveform generator. The cycle number can be adjusted. The excitation pulse spectrum with different cycle numbers is shown in Fig. 13. The cycle numbers of 6, 8, and 10 are chosen, which fall into the common range of values. It is clear that the more the number of cycles, the more the energy is concentrated at the center frequency. For different pulse cycle numbers, we observe the circumferential distribution of the signal at the axial position 300mm away from the transducer. The displacement amplitudes obtained in the simulation

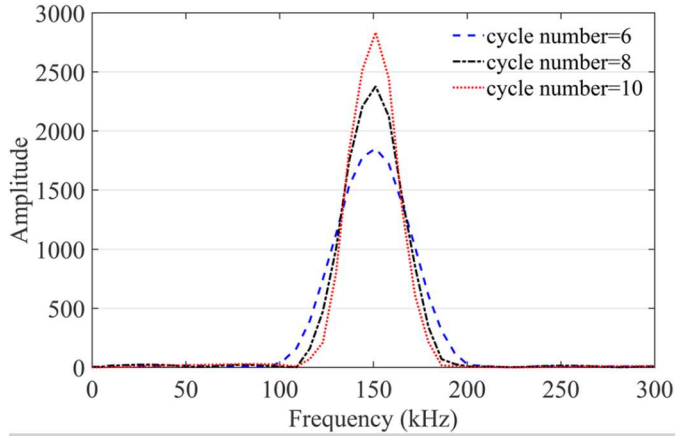

Fig. 13: The excitation pulse spectrum with different numbers of cycles.

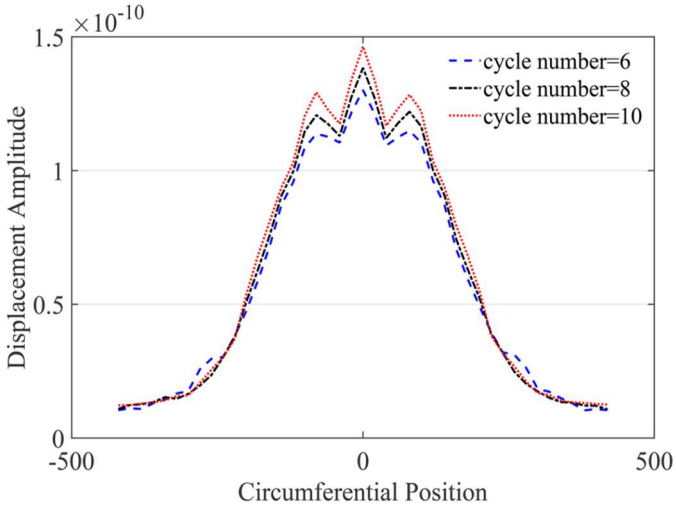

Fig. 14: The circumferential distribution of displacement with different pulse cycles.

are presented in Fig. 14. The other factors are kept the same. The corresponding experiments are also implemented, and the results show the same trend as in the simulation.

It can be seen that the larger the number of cycles, the larger the signal amplitude at the position directly in front of the transducer, but the increase in amplitude is slight. It is caused by the different energy values in the pulse with different cycle numbers. To get the half divergence angle, the amplitude is normalized and the extent of concentration is calculated. The half divergence angle for the three cycle numbers is 30.8°, 31.1°, and 31.4°, respectively. Thus, there is only a small increase in half divergence angle with more cycle numbers.

In addition, the small number of excitation pulse cycles means richer frequency components, and it is not suitable for exciting single-mode guided waves. It is worth noting that with a larger cycle number, the time duration of the pulse will increase and also the reflection wave. These will make it easier to cause the overlapping of the wavepackets.

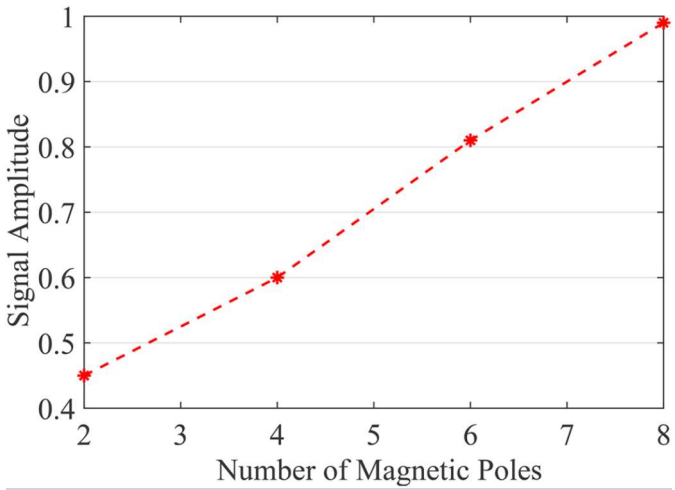

Fig. 15: The relation between the signal amplitude and the number of magnetic poles obtained in the experiment.

Thus, it will decrease the resolution of detection and increase the difficulty in identifying multiple close defects or features.

4. Number and central angle of magnetic poles

The designed transducer adopts magnets with the shape of a sector. Multiple magnetic poles are formed into an array to enhance the signal of the required mode and suppress the signals of other modes. The number of magnetic poles is changed to observe the variation of the received signal. Similarly, the size of the iron–nickel alloy belt is varied to match the magnet's parameter. The number of excitation pulse cycles is 6, and other factors are kept the same. Figure 15 shows the signal amplitude of the received signal in the experiments. Due to the wave superposition, the more number of magnetic poles leads to the higher amplitude of the ultrasonic signal. The relation between the amplitude and the magnetic pole number is nearly in the linear form. However, the time duration of the signal wavepacket will increase accordingly, which will have a negative impact on the subsequent time-of-flight extraction. Therefore, according to the actual requirements, the signal strength and the time duration of the wavepacket should be considered comprehensively to select the appropriate number of magnetic poles.

The central angle of the magnetic pole is the important factor to influence the wave propagation. The half divergence angle is calculated at an axial distance of 300mm in front of the transducer under different central angles. The results in the experiment and simulations are depicted in Fig. 16. It can be seen that as the central angle increases, the half divergence angle can be improved significantly. However, a larger central angle means a larger volume of the transducer. Thus, fewer transducers could be placed in the circumferential direction of the pipeline, which will decrease the ultrasonic wave density and further defect imaging resolution. The larger divergence angle is in contradiction with the imaging resolution to some extent. To achieve the required results, the compromise should be considered. In addition, larger magnets also bring higher manufacturing cost.

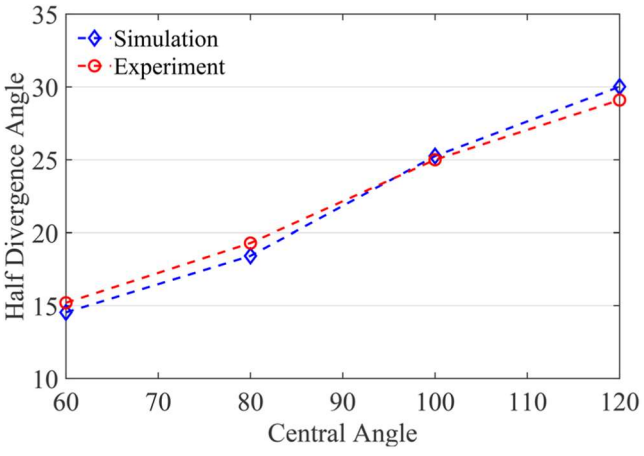

Fig. 15: The half divergence angle obtained in the simulation and experiment for different central angles of the magnetic pole.

V. CONCLUSION AND FUTURE WORK

In this work, a transducer for generating helical guided SH waves is designed and a corresponding characteristic analysis is conducted. The magnetostrictive effect is utilized in the transduction process. The transducer is composed of an iron–nickel alloy belt and sector magnets with wound copper wire. The theoretical analysis is provided to build the finite element model, and the half divergence angle is defined to evaluate the performance. The waveform in the simulation shows agreement with that obtained in the experiment. The frequency response characteristics indicate that the developed transducer works in the designed frequency. The magnetic field intensity attenuates quickly with the increase in the lift-off distance between the wire and the belt. The increase in excitation pulse cycle number leads to fewer frequency components and a slight rise in half divergence angle. The greater number of magnetic poles can enhance the signal amplitude, but it will lead to longer time durations of wavepackets. The central angle of the magnet influences the half divergence angle significantly. However, the larger central angle results in fewer transducers that could be distributed in the pipeline circumference. In future work, the detectability of the developed transducer will be investigated and the corresponding defect inspection will be employed.

ACKNOWLEDGMENTS

This research was financially supported by the National Key Research and Development Program of China (Grant No. 2018YFF0214701) and National Natural Science Foundation of China (NSFC) (Grant Nos. 51677093 and 51777100).

DATA AVAILABILITY

The data that support the findings of this study are available from the corresponding author upon reasonable request.

REFERENCES

[1]D. Alleyne and P. Cawley, "The long range detection of corrosion in pipes using Lamb waves," in *Review of Progress in Quantitative Nondestructive Evaluation, Review of Progress in Quantitative Nondestructive Evaluation* (Springer, 1995), pp. 2073–2080.
[2]J. J. da Silva, M. Goncalves Wanzeller, P. de Almeida Farias, and J. S. da Rocha Neto, "Development of circuits for excitation and reception in ultrasonic transducers for generation of guided waves in hollow cylinders for fouling detection," IEEE Trans. Instrum. Meas. **57**, 1149–1153 (2008).
[3]J. He, C. Zhou, L. Yang, and X. Sun, "Research on pipeline damage imaging technology based on ultrasonic guided waves," Shock Vib. **2019**, 1–18.
[4]H. Qi, J. Ye, X. Zhang, and H. Chen, "Wireless tracking and locating system for in-pipe robot," Sens. Actuators, A **159**, 117–125 (2010).
[5]X. Zhao, V. K. Varma, G. Mei, B. Ayhan, and C. Kwan, "In-line nondestructive inspection of mechanical dents on pipelines with guided shear horizontal wave electromagnetic acoustic transducers," J. Pressure Vessel Technol. **127**, 304–309 (2005).
[6]Z. Sun, A. Sun, and B.-F. Ju, "Deconvolution imaging of weak reflective pipe defects using guided-wave signals captured by a scanning receiver," Rev. Sci. Instrum. **88**, 024904 (2017).
[7]Z. Wang, S. Huang, S. Wang, S. Zhuang, Q. Wang, and W. Zhao, "Compressed sensing method for health monitoring of pipelines based on guided wave inspection," IEEE Trans. Instrum. Meas. **69**, 4722–4731 (2020).

[8]T. Nara, M. Fujieda, and Y. Gotoh, "Non-destructive inspection of ferromagnetic pipes based on the discrete Fourier coefficients of magnetic flux leakage," J. Appl. Phys. **115**, 17E509 (2014).
[9]T. R. Hay and J. L. Rose, "Flexible PVDF comb transducers for excitation of axisymmetric guided waves in pipe," Sens. Actuators, A **100**, 18–23 (2002).
[10]Y. Zhang, S. L. Huang, S. Wang, and W. Zhao, "Time-frequency energy density precipitation method for time-of-flight extraction of narrowband Lamb wave detection signals," Rev. Sci. Instrum. **87**, 054702 (2016).
[11]M. Hirao and H. Ogi, EMATs for Science and Industry: Noncontacting Ultrasonic Measurements (Springer Science & Business Media, 2013).
[12]R. Benegal, F. Karimi, T. Filleter, and A. N. Sinclair, "Optimization of periodic permanent magnet configuration in Lorentz-force EMATs," Res. Nondestr. Eval. **29**, 95–108 (2018).
[13]C. Pei, S. Zhao, P. Xiao, and Z. Chen, "A modified meander-line-coil EMAT design for signal amplitude enhancement," Sens. Actuators, A **247**, 539–546 (2016).
[14]G. Liu and J. Qu, "Guided circumferential waves in a circular annulus," J. Appl. Mech. **65**, 424–430 (1998).
[15]X. Zhao and J. L. Rose, "Guided circumferential shear horizontal waves in an isotropic hollow cylinder," J. Acoust. Soc. Am. **115**, 1912–1916 (2004).
[16]S. Wang, S. Huang, W. Zhao, and Z. Wei, "3D modeling of circumferential SH guided waves in pipeline for axial cracking detection in ILI tools," Ultrasonics **56**, 325–331 (2015).
[17]W. Luo, J. L. Rose, and H. Kwun, "A two dimensional model for crack sizing in pipes," AIP Conf. Proc. **700**, 187–192 (2004).
[18]W. Luo, J. L. Rose, and H. Kwun, "Circumferential shear horizontal wave axialcrack sizing in pipes," Res. Nondestr. Eval. **15**, 149–171 (2005).
[19]M. Hirao and H. Ogi, "An SH-wave EMAT technique for gas pipeline inspection," NDT E Int. **32**, 127–132 (1999).
[20]H. W. Kim, Y. E. Kwon, S. H. Cho, and Y. Y. Kim, "Shear-horizontal wave-based pipe damage inspection by arrays of segmented magnetostrictive patches," IEEE Trans. Ultrason., Ferroelectr., Freq. Control **58**, 2689–2698 (2011).
[21]H. W. Kim, H. J. Lee, and Y. Y. Kim, "Health monitoring of axially-cracked pipes by using helically propagating shear-horizontal waves," NDT&E Int. **46**, 115–121 (2012).
[22]W. Ren, J. He, S. Dixon, and K. Xu, "Enhancement of EMAT's efficiency by using silicon steel laminations back-plate," Sens. Actuators, A **274**, 189–198 (2018).
[23]Z. Wang, S. Huang, S. Wang, Q. Wang, and W. Zhao, "Design of electromagnetic acoustic transducer for helical lamb wave with concentrated beam," IEEE Sens. J. **20**, 6305–6313 (2020).
[24]Z. Wang, S. Wang, Q. Wang, W. Zhao, and S. Huang, "Development of a helical lamb wave electromagnetic acoustic transducer for pipeline inspection," IEEE Sens. J. **20**, 9715–9723 (2020).
[25]R. B. Thompson, "Physical principles of measurements with EMAT transducers," Phys. Acoust. **19**, 157–200 (1990).
[26]H. Ogi, "Field dependence of coupling efficiency between electromagnetic field and ultrasonic bulk waves," J. Appl. Phys. **82**, 3940–3949 (1997).
[27]X. Wan, G. Xu, Q. Zhang, P. W. Tse, and H. Tan, "A quantitative method for evaluating numerical simulation accuracy of time-transient Lamb wave propagation with its applications to selecting appropriate element size and time step," Ultrasonics **64**, 25–42 (2016).
[28]D. C. Jiles, "Theory of the magnetomechanical effect," J. Phys. D: Appl. Phys. **28**, 1537 (1995).
[29]R. B. Thompson, "A model for the electromagnetic generation and detection of Rayleigh and Lamb waves," IEEE Trans. Sonics Ultrason. **20**, 340–346 (1973).
[30]M. J. Sablik and S. W. Rubin, "Modeling magnetostrictive generation of elastic waves in steel pipes, I. Theory," Int. J. Appl. Electromagn. Mech. **10**, 143–166 (1999).
[31]M. J. Sablik, Y. Lu, and G. L. Burkhardt, "Modeling magnetostrictive generation of elastic waves in steel pipes, II. Comparison to experiment," Int. J. Appl. Electromagn. Mech. **10**, 167–176 (1999).
[32]Z. Wei, S. Huang, S. Wang, and W. Zhao, "Magnetostriction-based omnidirectional guided wave transducer for high-accuracy tomography of steel plate defects," IEEE Sens. J. **15**, 6549–6558 (2015).